Disordered strictly jammed binary sphere packings attain an anomalously large range of densities

Adam B. Hopkins and Frank H. Stillinger
Department of Chemistry, Princeton University, Princeton, New Jersey 08544, USA

Salvatore Torquato
Department of Chemistry, Princeton Institute for the Science and Technology of Materials, Department of Physics, Princeton Center for Theoretical Science, Program in Applied and Computational Mathematics, Princeton University, Princeton, New Jersey 08544, USA

(Received 9 May 2013; published 30 August 2013)

Previous attempts to simulate disordered binary sphere packings have been limited in producing mechanically stable, isostatic packings across a broad spectrum of packing fractions. Here we report that disordered strictly jammed binary packings (packings that remain mechanically stable under general shear deformations and compressions) can be produced with an anomalously large range of average packing fractions $0.634 \leqslant \phi \leqslant 0.829$ for small to large sphere radius ratios α restricted to $\alpha \geqslant 0.100$. Surprisingly, this range of average packing fractions is obtained for packings containing a subset of spheres (called the backbone) that are *exactly* strictly jammed, *exactly* isostatic, and also generated from *random initial conditions*. Additionally, the average packing fractions of these packings at certain α and small sphere relative number concentrations x approach those of the corresponding densest known *ordered* packings. These findings suggest for entropic reasons that these high-density disordered packings should be good glass formers and that they may be easy to prepare experimentally. We also identify an unusual feature of the packing fraction of jammed backbones (packings with rattlers excluded). The backbone packing fraction is about 0.624 over the majority of the α-x plane, even when large numbers of small spheres are present in the backbone. Over the (relatively small) area of the α-x plane where the backbone is not roughly constant, we find that backbone packing fractions range from about 0.606 to 0.829, with the volume of rattler spheres comprising between 1.6% and 26.9% of total sphere volume. To generate isostatic strictly jammed packings, we use an implementation of the Torquato-Jiao sequential linear programming algorithm [Phys. Rev. E **82**, 061302 (2010)], which is an efficient producer of inherent structures (mechanically stable configurations at the local maxima in the density landscape). The identification and explicit construction of binary packings with such high packing fractions could have important practical implications for granular composites where density is critical both to material properties and fabrication cost, including for solid propellants, concrete, and ceramics. The densities and structures of jammed binary packings at various α and x are also relevant to the formation of a glass phase in multicomponent metallic systems.

DOI: 10.1103/PhysRevE.88.022205 PACS number(s): 45.70.−n, 63.50.Gh, 61.66.Dk, 61.43.Dq

I. INTRODUCTION

A packing is an arrangement of nonoverlapping objects in a space of given dimension d, and the packing fraction ϕ is the fraction of the space that the objects cover. Packings of identical spheres have been employed in three-dimensional Euclidean space $\mathbb{R}^3$ to describe the structures and some fundamental properties of a diverse range of substances from crystals and colloids to liquids, suspensions and particulate media, amorphous solids, and glasses [1–7]. Complex structures with high symmetry can arise in packings of identical spheres through simple principles like density maximization in both confined and infinite spaces [8–21]. Polydisperse sphere packings have been studied recently as models for metallic glasses, in particular as packing effects are crucial in determining the ability of a metallic multicomponent atomic system to form a glass [1,22]. Packings of identical nonspherical objects in $\mathbb{R}^3$ have also been studied, though not to the extent of sphere packings, and have applications, for example, in the self-assembly of colloids and nanoparticles [23–35]. In structural biology, molecular dynamics simulations of interactions between large numbers of molecules employ chains of identical nonoverlapping spheres as models for various biological structures such as proteins and lipids [36–38], and packing of nonspherical objects of different sizes are used, for example, in tumor growth modeling [39–41].

Experimental packings of oiled steel ball bearings originally led to the idea that mechanically stable random packings of identical spheres could not exhibit packing fractions exceeding 0.64 or declining below 0.60 [42,43]. In particular, the notion of a "random close packing" (RCP) state for monodisperse hard spheres was pioneered by Bernal [44,45] and has a venerable history [46,47]. The RCP state is thought to be the *maximal* packing fraction that a large random collection of congruent identical spheres can attain, and this packing fraction of about 0.64 is thought to be a universal quantity. Mathematically constructed models [48] and early computer simulations [49] seemed to support these conclusions, though later work demonstrated that the limiting packing fractions obtained were highly dependent on the packing protocols [5,47,50–55]. Moreover, "random" was never defined, and because infinitesimal increases in ϕ above 0.64 would be accompanied by undetectable changes in what might be considered "randomness," the RCP concept has been challenged [5,47,53–55].

It has been suggested that the notion of a RCP state for hard spheres be supplanted by the mathematically precisely defined maximally random jammed (MRJ) state [53,54]. Maximally random jammed packings are those that exhibit the least order,

as measured by a variety of different order metrics, from the set of all strictly jammed (mechanically stable) packings [13,54]. In contrast to empirical RCP states, MRJ packings have unique properties. In particular, three-dimensional MRJ packings have a well-defined packing fraction ϕ_{MRJ} in the infinite-volume limit, and the jammed spheres in an MRJ packing are *isostatic* [33,53], meaning that the average number of contacts per jammed sphere is the minimum required for mechanical stability [56]. Additionally, the pair correlation functions $g_2(r)$ of MRJ packings decay to unity proportionally to $-1/r^4$ as $r \to \infty$, with corresponding linear behavior of the structure factor $S(k)$ as $k \to 0$ [57,58], which implies hyperuniformity [59]. This linear behavior in the structure factor has been experimentally observed in colloids [34], granular materials [60], and amorphous silicon [61,62]. Furthermore, it has been used to extract growing length scales in million-particle packings of monodisperse spheres [58] as packing fraction approaches jamming and in models of supercooled glassy atomic systems [63] as temperature is decreased.

In a strictly jammed packing, no simultaneous collective motion of the objects and non-volume-increasing deformation of the unit cell can reduce density, meaning that all strictly jammed packings are mechanically stable. Generally, such a packing consists of a subset of spheres, called the *backbone*, that is strictly jammed, and a number of *rattlers* that can be displaced without displacing (or overlapping) any neighbors. The packing fraction at which a packing becomes strictly jammed and the degree of disorder, or "randomness," in a packing [13,54,59,64–67] are highly dependent on the specifics of the packing protocol, including the initial configuration and density before compression is begun, compression rate, and system dynamics [47,68]. This means that though all MRJ packings are strictly jammed, not all strictly jammed disordered packings are MRJ [69], since MRJ packings additionally require minimal order and exhibit characteristics such as isostaticity.

Similarly to monodisperse sphere packings, at each specified pair of small to large sphere size ratio α and small sphere relative number concentration x, MRJ *binary* sphere packings, or packings of spheres of only two sizes, are expected to exhibit a well-defined packing fraction $\phi_{\mathrm{MRJ}}(\alpha,x)$ and exact isostaticity of their jammed backbones. However, by spanning over the α-x parameter space, the possible range of $\phi_{\mathrm{MRJ}}(\alpha,x)$ may be surprisingly large; one of the aims of this paper is to explore the extent of this range. For example, it was recently shown that the maximal packing fractions of *ordered* binary sphere packings over a large set of α and x is substantially greater than was previously known [20,70,71].

In this work, we generate and analyze disordered, strictly jammed binary sphere packings of $N = 1000$ to $N = 15\,000$ spheres at various $\alpha \geqslant 0.100$ and $0 \leqslant x \leqslant 1$ where each packing contains an exactly isostatic backbone. We are able to construct such packings with high fidelity using the Torquato-Jiao (TJ) sequential linear programming algorithm [20,70,72], a packing protocol that is particularly well suited to constructing strictly jammed, isostatic packings, for reasons that will be discussed in detail later in this work. We find that for $\alpha \geqslant 0.100$ and $0 \leqslant x \leqslant 1$, strictly jammed binary sphere packings with exactly isostatic backbones exhibit an anomalously large range $0.634 \leqslant \phi_{\mathrm{MRJ}}(\alpha,x) \leqslant 0.829$ of average packing fractions and

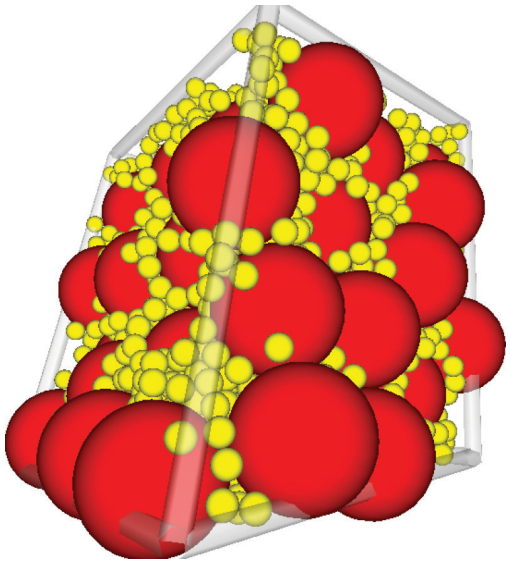

FIG. 1. (Color online) Depiction of a 2000-sphere unit cell of a periodic strictly jammed binary packing at $\alpha = 0.200$ and $x = 0.970$ with packing fraction $\phi = 0.785$. This MRJ packing was generated using the Torquato-Jiao (TJ) algorithm and contains an exactly isostatic backbone for strict jamming with an average of 6.0035 contacts per jammed sphere (see definition in text). The packing contains 288 rattlers (all small spheres) to an accuracy of 10^{-6} large-sphere diameters.

that for certain values of α and x, $\phi_{\mathrm{MRJ}}(\alpha,x)$ approaches the density of the densest known *ordered* packings [20,70]. These are particularly unexpected findings considering that the packings are generated without any sort of special preparation from random sequential addition (RSA) initial conditions [5] at low initial packing fractions $0.1 \leqslant \phi_{\mathrm{init}} \leqslant 0.3$. Figure 1 is an image of a 2000-sphere isostatic packing at $\phi = 0.785$ with $\alpha = 0.200$ and $x = 0.970$.

Past investigations [69,72] have employed the TJ algorithm to study strictly jammed packings of disordered monodisperse spheres, but in this work we apply the algorithm to disordered *binary* sphere packings. The packings that we have generated are MRJ like due to the nature of the TJ algorithm [72] and the use of RSA initial conditions. This is also evidenced by the *exact* isostaticity of both the monodisperse and binary disordered jammed packings studied here and the forms of their corresponding pair correlation functions. We therefore refer to the packings hereafter simply as MRJ [as indicated by the terminology $\phi_{\mathrm{MRJ}}(\alpha,x)$], deferring a detailed study of structural disorder employing order metrics to a future work due to the challenging requirement of defining and discussing order metrics that are applicable across the entire α-x plane of disordered and ordered binary packings.

Previously, research into simulated disordered binary sphere packings had not focused on mechanical stability because it was difficult not only to simulate strictly jammed packings but even to conclusively demonstrate strict jamming [56,73]. Consequently, many previous simulation studies of disordered binary sphere packings have produced packings that are not mechanically stable [74–76] and report *coordination* as opposed to *contact* numbers, where a coordination

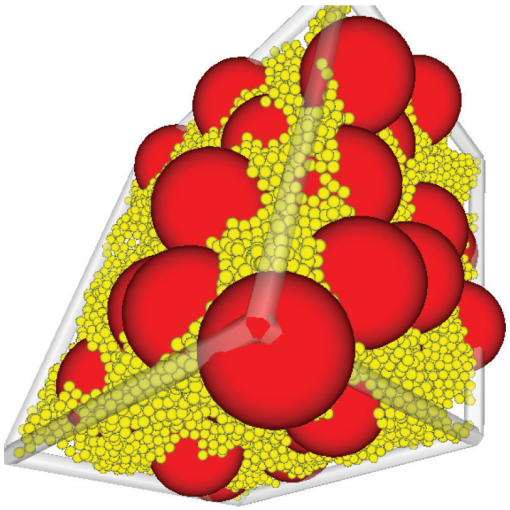

FIG. 2. (Color online) Depiction of a 15 000-sphere unit cell of a periodic strictly jammed binary packing at $\alpha = 0.100$ and $x = 0.9968$ with packing fraction $\phi = 0.829176\ldots$. This MRJ packing was generated using the Torquato-Jiao (TJ) algorithm and exhibits an exactly isostatic backbone. The packing contains 14 954 rattlers (14 952 small and 2 large) to an accuracy of 10^{-12} large sphere diameters (the number of rattlers calculated is identical from contact tolerances of 10^{-12} to 10^{-5} large sphere diameters). The jammed backbone of this packing, consisting of 46 large spheres, exhibits a packing fraction of $0.605892\ldots$. It is expected that greater packing fractions at $\alpha = 0.100$ for packings at slightly larger values of x can be achieved, since for the other values of α studied, the greatest packing fraction as a function of x was achieved for packings where the vast majority of small spheres were present in the packing backbone (i.e., were not rattlers).

number indicates only proximity of two spheres, whereas a *contact* number reflects mechanical stability and is derived from a jammed network [73]. It is perhaps for these reasons that previous studies found maximal packing fractions for disordered binary packings at ranges of α down to $\alpha = 0.100$ of only about 0.79 [55], whereas we find strictly jammed, exactly isostatic sphere packings generated from RSA initial conditions with packing fractions up to 0.829. Figure 2 is an image of a 15 000-sphere packing with exactly isostatic backbone consisting of 48 large and 14 952 small spheres ($x = 0.9968$) with packing fraction $\phi_{\mathrm{MRJ}}(0.100,0.9968) = 0.829176\ldots$.

Experimental studies of binary sphere packings, employing, for example, binary spherical colloids [77] and metal shot [78], produce mechanically stable packings by design. However, it is difficult in experimental setups to identify rattlers or even average coordination numbers and, therefore, to precisely measure packing characteristics such as average number of contacts per sphere $\bar{z}$. Further, physical experiments can be influenced not only by packing protocol but also by factors that can be removed from simulations, including physical packing boundaries, friction, the relative densities of small and large spheres, and aberrations away from perfect sphericity. Past experiments with binary sphere packings yielded density ranges of about $\phi = 0.64$ to $\phi = 0.77$ for $\alpha \geqslant 0.1$ [77,78].

In contrast, the TJ algorithm [20,70,72] is particularly well suited to study disordered packings of spheres due to its capability to produce mechanically stable packings where contacts between spheres (and therefore rattlers) can be precisely identified to arbitrary numerical precision. This capability is particularly noteworthy, since no other sphere-packing algorithm known to the authors consistently produces *exact* isostaticity or even strictly jammed packings. This is a crucial point, as recent works [68,79] studying monodisperse and binary sphere packings at jamming have concluded that isostatic jammed packings of spheres occur over a range of packing fractions. It is important to note that because such packings were not tested for exact isostaticity or strict jamming, it is not clear that this conclusion is valid, especially in the infinite-volume limit. In our investigations, though we find a small range of packing fractions for strictly jammed, exactly isostatic packings of a finite number of spheres at each specified α and x, this range decreases apparently to zero as the size of the packing increases. This issue as well as higher-order rattler statistics is the subject of an analogous study of MRJ monodisperse spheres under strict jamming [80].

In the first part of this paper, we present the packing fractions of isostatic binary sphere packings produced using the TJ algorithm across a range of x and $\alpha \geqslant 0.100$. We also discuss the average number and types of contacts between jammed spheres in these packings, and the criteria for determining whether a sphere is a rattler.

We then examine the trends in average density as a function of x at fixed α. The qualitative "triangular" shape of density as a function of x is observed [74–76,81]; however, we find proportionality of $\phi_{\mathrm{MRJ}}(\alpha,x)$ according to $a + bx/(c - x)$ with a, b, and c constants, where, for example, at $\alpha = 0.200$ this proportionality ranges from $x = 0$ to the observed maximum at $x = 0.970$. In addition, for all values of α, we find that the packing fraction of the jammed backbone remains nearly constant at about $\phi = 0.624$ from $x = 0$ up to a value of x, dependent on α, near which $\phi_{\mathrm{MRJ}}(\alpha,x)$ reaches a maximum. We also identify a drop in average relative percentage of small rattlers as a function of x at fixed α that precedes the peak in density.

Next, we present pair correlation functions $g_2(r)$, with r the radial distance between pairs of sphere centers. We discuss fundamental changes in pair correlation functions that emerge as x is varied at fixed α. Finally, we summarize our results and discuss potential applications of our findings to the production of solid propellants, concrete, and ceramics.

II. BINARY MRJ PACKINGS WITH ANOMALOUSLY LARGE DENSITY RANGES

There have been numerous algorithmic protocols used to simulate dense packings of identical spheres. For example, the Lubachevsky-Stillinger (LS) protocol [50] simulates frictionless spheres within a periodic unit cell that act according to Newtonian dynamics while undergoing elastic collisions and growing at a constant rate Γ. Research using the LS algorithm demonstrates that when the growth rate is fast, jammed disordered roughly isostatic packings can be produced [57,82]. The packing fractions ϕ of these packings are strongly dependent on the growth rate and initial conditions, as are average contact numbers $\bar{z}$, with ϕ and $\bar{z}$ tending to increase with decreasing growth rate Γ. In general, research has shown

that the packing fraction of jammed, disordered identical spheres is strongly dependent on packing protocol [47]. However, the packing fraction of MRJ packings appears to be somewhere between 0.63 and 0.64, as determined using the LS protocol for very fast growth rates [53,83].

Though the LS algorithm can be used to generate strictly jammed sphere packings, for large numbers of spheres and fast growth rates, pressure (and therefore simulation time) tends to diverge before a strictly jammed packing is produced. Using the TJ algorithm to quickly generate packings can be thought of as similar to using the LS algorithm with an extremely fast growth rate, except that the resultant packings are guaranteed to be strictly jammed. This is because the TJ algorithm exactly solves for the linear movement of the unit cell and collective motion of the spheres that maximizes density.

Limiting the TJ algorithm at each step to small displacements in sphere position (less than 0.001 large sphere diameters) and unit cell shape, only localized adjustments to sphere positions are possible. This means that each step in the TJ algorithm gives a solution for local improvements in density that is similar to (but far more efficient than) the process by which quickly compressed (or cooled) physical systems exhibiting strong repulsive pair potentials densify when there is not enough time to equilibrate. It therefore is not surprising that for $N = 1000$ spheres, the TJ algorithm produces isostatic jammed packings of identical spheres with packing fractions of $\phi = 0.6336 \pm 0.0018$, very similar [83] to the packing fractions obtained for MRJ packings using the LS algorithm [84]. It is noteworthy that scalar order metrics give nearly identical averaged values for these packings and MRJ packings produced using the LS protocol.

It is surprising to find that the range of average packing fractions of binary MRJ structures for $x \in [0,1]$ and $\alpha \geqslant 0.100$ obtained using the TJ algorithm and RSA initial conditions is $0.634 \leqslant \phi \leqslant 0.829$. The lower limit is obtained for monodisperse packings, i.e., at any value of α with $x = 0$ or, equivalently, $x = 1$. However, by removing the rattlers from binary MRJ packings and considering only their backbones, even lower packing fractions can be obtained while preserving strict jamming and exact isostaticity.

Due to the requirement of mechanical stability, disordered strictly jammed structures require a nonzero minimum density; for example, in $\mathbb{R}^3$ for identical spheres, disordered strictly jammed packings have been produced with packing fractions no lower than 0.60 [72], and *ordered* strictly jammed packings have been produced with packing fractions as low as $\sqrt{2}\pi/9 \approx 0.494$ [85]. For the disordered binary packings studied at $\alpha = 0.100$, 0.150, 0.200, and 0.330, a decrease in the average packing fraction of the jammed backbones as a function of x at fixed α is observed when x is only slightly smaller than the value for which the maximum packing fraction (including rattlers) is obtained. The lowest average packing fraction $\phi = 0.606$ of jammed backbones of MRJ packings appears as a local minimum in x at $x = 0.9968$ with α fixed at $\alpha = 0.100$. For the other values of α studied, this local minimum in the average packing fraction of the jammed backbones is less pronounced and occurs at somewhat smaller values of x.

Table I presents the highest packing fractions $\phi_{\mathrm{MRJ}}(\alpha,x)$ obtained for binary MRJ structures using the TJ algorithm. We expect these highest $\phi_{\mathrm{MRJ}}(\alpha,x)$ to increase at values of α smaller than 0.100. We also expect the the minimal packing fraction of the jammed backbones of MRJ binary packings to decrease for $\alpha \leqslant 0.100$.

TABLE I. Highest average packing fractions of binary MRJ packings obtained using the TJ algorithm

α	Highest $\phi_{\mathrm{MRJ}}(\alpha,x)$
0.100	$\phi_{\mathrm{MRJ}}(0.100,0.997) = 0.829$
0.150	$\phi_{\mathrm{MRJ}}(0.150,0.989) = 0.806$
0.200	$\phi_{\mathrm{MRJ}}(0.200,0.97) = 0.785$
0.330	$\phi_{\mathrm{MRJ}}(0.330,0.90) = 0.718$
0.450	$\phi_{\mathrm{MRJ}}(0.450,0.80) = 0.682$
0.950	$\phi_{\mathrm{MRJ}}(0.950,0.045) = 0.635$

Producing isostatic jammed sphere packings is nontrivial, yet the TJ algorithm consistently generates strictly jammed, exactly isostatic packings. The total number of contacts $Z(N)$ necessary for a packing in a finite-sized deformable unit cell to be strictly jammed is [56]

$$Z(N) = 3N + 3. \tag{1}$$

All packings that we produce using the TJ algorithm include this number (a small percentage include one more than this number, presumably because the numerical tolerance of the simulation was not sufficient to distinguish between proximity and contact, but these packings are excluded from our results). For collective jamming, jamming of a bounded packing of finite size where there is no unit cell to deform, only $3N - 2$ contacts are required for jamming in three dimensions.

The reason leading to this requirement [Eq. (1)] is subtle and requires a more detailed explanation. The total number of contacts $3N + 3$, or $6 + 6/N$ average contacting spheres per given sphere, is required such that all degrees of freedom available to the spheres in the packing be restricted by contacts. There are dN degrees of translational freedom available to the spheres, and $d(d+1)/2$ degrees of symmetric shear and strain freedom available to the periodic box in which the spheres are placed. A total of d degrees of freedom are subtracted to remove arbitrary translations of the box and spheres in space (which do not result in unjamming) and an additional single degree of freedom is subtracted as deformations of the box are required to be non-volume-increasing. A single degree of freedom is then added back, which can be best explained by noting that a trapping simplex in d-dimensional configuration spaces requires $d + 1$ bounding hypersurfaces, which equates to $d + 1$ sphere contacts. The total, $d(N-1) + d(d+1)/2 - 1 + 1$, is equal to $3N + 3$ in three dimensions.

To check if the backbone of a strictly jammed packing is isostatic, it is necessary to determine which spheres in the packing are rattlers, for which purpose we employ an iterative scheme. First, the total contacts between all spheres are counted and tabulated, employing a specified contact tolerance t, and local jamming is checked using the linear programming method described by Donev *et al.* [73]. Those spheres that are not locally jammed are labeled rattlers. Next, we repeat this scheme after removing all contacts involving spheres identified as rattlers and continue repeating until no new rattlers are identified. Figure 3 is a plot of the number of rattlers identified in a packing of 1000 spheres

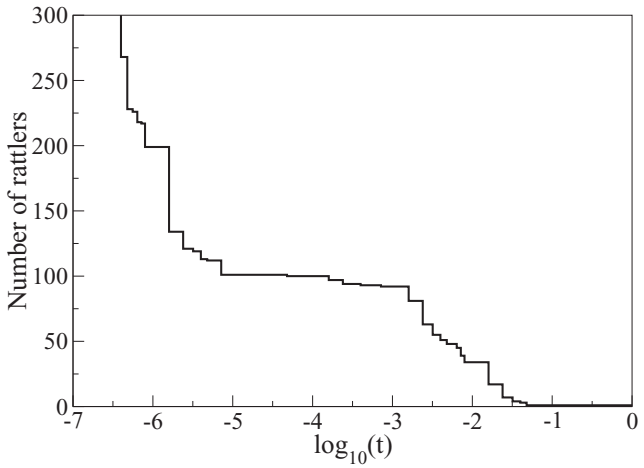

FIG. 3. Plot of the number of rattlers identified as a function of contact tolerance t (with t in units of large sphere diameters) for a packing of 1000 spheres at $\alpha = 0.45$ and $x = 0.850$, where in this packing the TJ algorithm has been directed to solve to a numerical contact tolerance of 8×10^{-6}. Note the "plateau" beginning just before the algorithm's numerical contact tolerance 7×10^{-6} and spanning about an order of magnitude to 5×10^{-5}, indicating that all rattlers have been identified to the precision solved by the algorithm. At $t = 7 \times 10^{-6}$, there are exactly 101 rattlers and an average of 6.0067 contacts per jammed sphere, precisely the number required for isostaticity.

at $\alpha = 0.450$, $x = 0.850$ as a function of the contact tolerance t in the rattler-identification algorithm. The plot illustrates the contact tolerance for strict jamming as solved for by the TJ algorithm, which coincides with the contact tolerance of the rattler-identification algorithm over a "plateau" of a constant number of rattlers identified, as seen in Fig. 3.

III. TRENDS IN DENSITY AND NUMBER OF RATTLERS

In addition to studying the packing fractions of MRJ binary packings, we have also studied the functional form of $\phi_{\mathrm{MRJ}}(\alpha,x)$ as a function of x at fixed α, the composition of small and large spheres present in the jammed backbone, and the number of small and large rattlers. We find that for all α studied, $\phi_{\mathrm{MRJ}}(\alpha,x)$ at fixed α can be described at all values of x by two functional forms, that the packing fraction of the jammed backbone remains nearly constant at about $\phi = 0.624$ for all values of α at the vast majority of values of x, and that small spheres are present in the jammed backbone at all values of $0 < x < 1$ and $\alpha \geqslant 0.150$ (for some of the strictly jammed packings studied at $\alpha = 0.100$, all small spheres were rattlers).

Past research has identified a qualitative "triangular" shape in the dependence of $\phi_{\mathrm{MRJ}}(\alpha,x)$ on x at fixed α, and our work supports this finding. However, more precisely, we find proportionality of packing fraction with $a + bx/(c - x)$ at $\alpha = 0.100$, 0.150, 0.200, 0.330, and 0.450 from $x = 0$ to a certain value of x, $x = x_0(\alpha)$ [where $x_0(\alpha)$ is not necessarily the maximum of $\phi_{\mathrm{MRJ}}(\alpha,x)$]. The functional form found can be explicitly written as

$$\phi_{\mathrm{MRJ}}(\alpha,x) = a + \frac{b(\alpha)x}{c(\alpha) - x}; \quad x \leqslant x_0(\alpha). \tag{2}$$

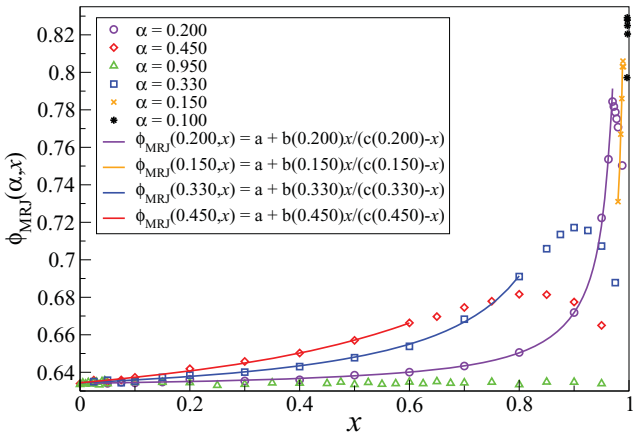

FIG. 4. (Color online) Plot of the average packing fraction obtained at various values of x and $\alpha = 0.100$, 0.150, 0.200, 0.330, 0.450, and 0.950, where each data point except at $\alpha = 0.100$ represents an average of 10 packings (the measured standard deviation is slightly smaller than the size of the symbols). For $\alpha = 0.100$, due to computational time constraints, each data point represents a single packing. No fewer than 40 large spheres are present in any packing. The solid curves for $\alpha = 0.150$, 0.200, 0.330, and 0.450 are least-squares fits $\phi_{\mathrm{MRJ}}(\alpha,x) = a + b(\alpha)x/[c(\alpha) - x]$ with R^2 values of 0.9992, 0.9998, 0.9976, and 0.9958, respectively, where the fits range over the values of x indicated by the curves. We do not display curves for $\alpha = 0.100$ due to a paucity of data and for $\alpha = 0.950$ due to the inability to define a value $x_0(0.950)$.

For $\alpha = 0.950$, no value $x_0(\alpha)$ can be identified, as $\phi_{\mathrm{MRJ}}(\alpha,x)$ is roughly flat over all values of x studied. We additionally note that the functional form of Eq. (2) applied to the data at $\alpha = 0.100$ and 0.150 is limited to the small number of values of x studied, $0.98 \leqslant x \leqslant 0.99$ for $x = 0.150$ and $0.996 \leqslant x \leqslant 0.997$ for $\alpha = 0.100$. Limited ranges of x are studied at $\alpha = 0.100$ and $\alpha = 0.150$ due to computational time constraints, as large numbers of 5000 to 15 000 spheres were necessary to carefully study packings near the peak in packing fraction of $\phi_{\mathrm{MRJ}}(\alpha,x)$ at these two values of α.

In Eq. (2), α can be read as a parameter that defines the constants $b(\alpha)$ and $c(\alpha)$. For $x > x_0(\alpha)$, we find that packing fraction is proportional roughly to a polynomial of degree 3. The behavior of $\phi_{\mathrm{MRJ}}(\alpha,x)$ as a function of x for six values of α is displayed in Fig. 4. Proportionality according to $a + bx/(c - x)$ up to $x_0(\alpha)$ leads to an increasingly sharp peak in $\phi_{\mathrm{MRJ}}(\alpha,x)$ with decreasing α, where we find, within the resolution in x of the study, that $x_0(\alpha)$ corresponds approximately with the peak in packing fraction for $\alpha = 0.100$, 0.150, and 0.200. Identifying such a sharp and pronounced peak in packing fraction as a function of x at small values of α is a surprising finding, indicating that the precise tailoring of the size and composition of mixtures of spherical composites can lead to substantial increases in density.

It is noteworthy that the densest known *ordered* packing at $\alpha = 0.200$, $x = 0.970$ has a packing fraction of 0.796, differing by only about 1.4% from $\phi_{\mathrm{MRJ}}(0.200, x = 0.970)$ [20,70]. The densest packing referenced is a *phase-separated* packing including the following: an (11-1) phase that can be described as a distorted fcc lattice of large spheres with 11 small spheres per large sphere in the interstices and a phase

of fcc small spheres. A diagram of the (11-1) structure can be found in Appendix A. It is conjectured that this proximity in maximal packing fractions between the densest ordered and MRJ packings also may be present at $\alpha = 0.150$ and $\alpha = 0.100$, but this cannot be confirmed at present since the densest ordered packings at these two smaller values of α has not been studied in detail. The proximity in densities between the MRJ and densest ordered packings at $\alpha = 0.200$ and $x = 0.970$ is striking. The small structural entropy difference (via free volume) between the two packing configurations and the additional entropy in the MRJ packings due to disorder indicate that (a) free energy is not significantly reduced by freezing and, therefore, that these are good parameters for generating binary sphere glasses and (b) that the MRJ packings at these α and x should be particularly easy to obtain experimentally.

The equality presented in Eq. (2) and Fig. 4 is also clearly present when $\phi_{\mathrm{MRJ}}(\alpha,x)$ is measured, as it often is [74–76], as a function of α and the *relative volume fraction* of small spheres x_V, where

$$x_V = \frac{x\alpha^3}{x\alpha^3 + 1 - x}. \tag{3}$$

Under the change of variables $x \to x_V$, Eq. (2) retains its functional form, i.e.,

$$\phi_{\mathrm{MRJ}}(\alpha,x_V) = a + \frac{b_V(\alpha)x_V}{c_V(\alpha) - x_V}, \tag{4}$$

with $b_V(\alpha) \equiv b(\alpha)/[1 + c(\alpha)\alpha^3 - c(\alpha)]$ and $c_V(\alpha) \equiv c(\alpha)\alpha^3/[1 + c(\alpha)\alpha^3 - c(\alpha)]$. Figure 5 is a plot of $\phi_{\mathrm{MRJ}}(\alpha,x_V)$

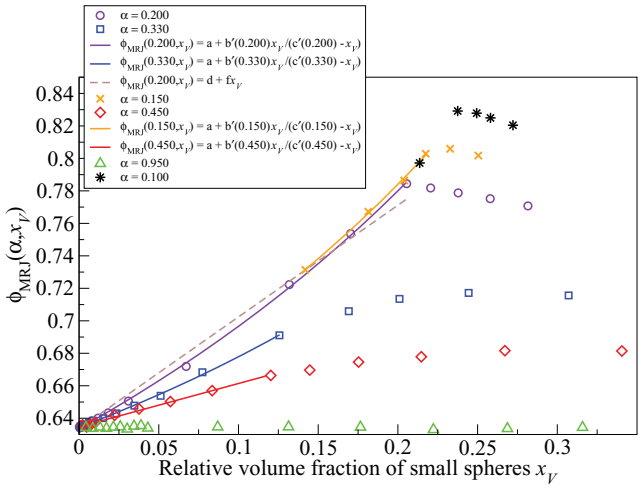

FIG. 5. (Color online) Plot of the average packing fraction $\phi_{\mathrm{MRJ}}(\alpha,x_V)$ versus x_V for the values of x presented in Fig. 4, alongside fits to the data according to Eq. (4) for $\alpha = 0.150$, 0.200, 0.330, and 0.450. Each data point represents an average of 10 packings where the measured standard deviation is close to the size of the symbols. For $\alpha = 0.100$, due to computational time constraints, each data point represents a single packing. The solid curves are least-squares fits of the form of Eq. (4) to the data from $x_V = 0$ to $x_V = x_V(x_0(\alpha))$, except for $\alpha = 0.150$, where the fit ranges over all available data, $0.1419 \leqslant x_V \leqslant x_V(x_0(0.150))$. The dashed line is a linear least-squares fit to the data for $\alpha = 0.200$ from $x_V = 0$ to $x_V(x_0(0.200))$, shown for comparative purposes only. It is visually clear from the plot that the linear fit to $\alpha = 0.200$ is a significantly less precise descriptor of the data than is the fit curve according to Eq. (4).

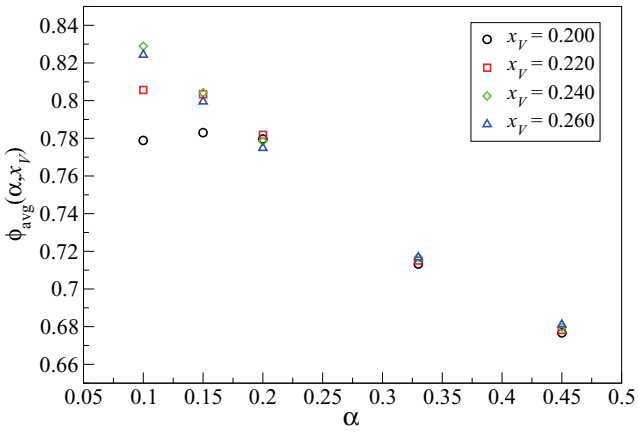

FIG. 6. (Color online) Plot of the average packing fraction $\phi_{\mathrm{MRJ}}(\alpha,x_V)$ versus α for $x_V = 0.200$, 0.220, 0.240, and 0.260. Each data point represents a linear extrapolation from the nearest values of x_V at which packings were produced, where the same packings used to create Figs. 4 and 5 are considered. The linear extrapolations extend no more than 6% from the closest value of x_V at which packings were produced.

for four values of α along with curves fit to the data from $x_V = 0$ to $x_V(x_0(\alpha))$, where the fit curves are of the form of Eq. (4). Figure 5 also includes a plot of the best linear fit to $\phi_{\mathrm{MRJ}}(0.200,x_V)$ from $x_V = 0$ to $x_V(x_0(0.200)) \approx 0.20$, clearly demonstrating visually that the form of Eq. (4) is a better fit than a line. All fit curves displayed in Fig. 5 according to Eq. (4) are better fits than a line, though the fit for $\alpha = 0.450$ is only slightly better than a line. Data and fit curves for $\alpha = 0.100$ and $\alpha = 0.950$ are not shown for the same reasons they were not shown in Fig. 4. Appendix B discusses other fits to the average packing fraction data obtained in this study.

Though the graphs displayed thus far all plot ϕ_{MRJ} as a function of x or x_V at fixed α, plots of ϕ_{MRJ} as a function of α at fixed x_V can also be drawn. Figure 6 displays $\phi_{\mathrm{MRJ}}(\alpha,x_V)$ as a function of α at fixed x_V for $x_V = 0.200$, 0.220, 0.240, and 0.260 for the values of α studied (excluding $\alpha = 0.950$ for visual clarity). The data presented are derived from the data presented in Figs. 4 and 5; since the packings studied were not generated at the precise values of x_V presented in Fig. 6, the data presented in the plot are linear extrapolations between the nearest two values of x_V at which packings were produced. Only four values of x_V are plotted so that these linear extrapolations extend minimally from values of x_V at which packings were actually produced.

Another interesting feature in the densities of the MRJ binary packings generated becomes apparent when packing fraction is calculated with all rattlers removed. In this case, we find that for the majority of the α-x plane, the average packing fraction of the backbones is about 0.624. This is an unexpected finding considering that at all values of α and x studied, small spheres contribute to the jammed backbones of packings (except at $\alpha = 0.100$) and are often more numerous than the large spheres. For example, at $\alpha = 0.330$ and $x = 0.800$ with $N = 1000$, we find the average jammed backbones to be comprised of an average of 231.8 small spheres and 199.6 large spheres, yielding an average packing fraction of 0.628.

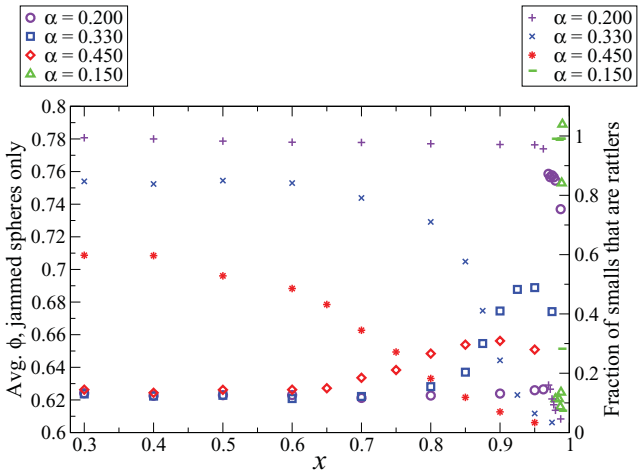

FIG. 7. (Color online) Average packing fraction of the jammed backbone obtained at various values of α and x (left axis and legend). The average packing fraction of the jammed backbone is roughly constant at 0.624 for the majority of the α-x plane, including over the area $x < 0.3$ not shown in the figure. Overlayed is a plot of the average relative percentage of small rattlers (right axis and legend). Note that this percentage is roughly constant over the same range of x at fixed α that the average packing fraction of the jammed backbones is roughly constant (at the value 0.624).

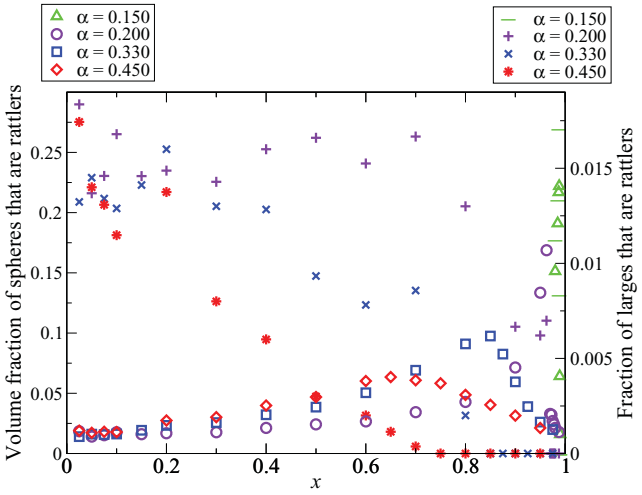

FIG. 8. (Color online) Average volume fraction of spheres that are rattlers obtained at various values of α and x (left axis and legend). For all values of α studied, as x increases from $x = 0$, the volume fraction of spheres that are rattlers increases to a maximum that is concurrent with the peak in the total packing fraction and then declines. Overlayed on the plot of the average volume fraction of spheres that are rattlers is a plot of the average number fraction of large spheres that are rattlers (right axis and legend).

Figure 7 plots the average packing fractions of the packings studied in Fig. 4 for four values of α, except with rattler spheres removed. Overlayed on this plot is a plot of the average fraction of small spheres that are rattlers. Data for fewer values of x were collected due to computational time constraints at $\alpha = 0.150$ and $\alpha = 0.100$, and, consequently, data for $\alpha = 0.100$ are not plotted in Fig. 7. However, the data for $\alpha = 0.100$ and $\alpha = 0.150$ show similar behavior to the data for the $\alpha = 0.200$ packings, except the sharpness of the increase in backbone packing fraction at the peak in density is more pronounced, as is the sharpness of the decrease in number of spheres that are rattlers. Data for $\alpha = 0.950$ are not plotted in Fig. 7, as, for all x studied, the backbone packing fraction and fraction of small spheres that are rattlers do not deviate substantially from the values taken for monodisperse packings.

Figure 7 also illustrates that the increase in the backbone packing fraction occurs concurrently with a drop in the relative percentage of small rattlers (all values of α studied display this trend except for $\alpha = 0.950$). The increase is additionally nearly concurrent with the complete disappearance of large rattlers, i.e., in not one of the thousands of packings studied was a single large rattler present past the beginning (roughly) of the rise in backbone packing fraction. These observations indicate a fundamental change in the underlying structure of MRJ binary sphere packings from (a) a jammed backbone of mostly large and some small spheres at a packing fraction of about 0.624, incorporating small rattler spheres in the interstices, to (b) a jammed backbone comprised of mostly small spheres incorporating a few small and no large rattlers.

Over the α-x plane for the packings studied, the total volume fraction of spheres that are rattlers varies substantially from its value for monodisperse packings of about 1.6% to as high as 26.9% at $\alpha = 0.100$, $x = 0.997$. Figure 8 illustrates trends in the volume fraction of spheres that are rattlers for the values of x studied at $\alpha = 0.450$, 0.330, 0.200, and 0.150. Alongside this data are plotted the fraction of large spheres that are rattlers at the same four values of α. The data for $\alpha = 0.100$ are not plotted due to data sparsity, but the data exhibit a qualitative trend similar to that of $\alpha = 0.200$ and $\alpha = 0.150$, except with a sharper peak exhibiting a maximum at roughly $x = 0.997$.

There were no small spheres present in the jammed backbones of the 15 000-sphere packings at $\alpha = 0.100$ and $x = 0.996$; however, we do not believe this observation to be representative of packings of all sizes at $\alpha = 0.100$ for $x \leqslant 0.996$. Rather, we suspect that packings of greater than 15 000 spheres at $x = 0.996$ will include small spheres in their jammed backbones and that they were absent in the packings studied because the jammed backbone included only 54 spheres. Comparing to the $\alpha = 0.150$ packings at values of x before the peak in the backbone packing fraction, at $x = 0.980$, small spheres represent about 6% of the jammed backbone by number, and at $x = 0.988$, they represent about 43%. This is in spite of the fact that the small spheres of diameter ratio $\alpha = 0.150$ are smaller than the largest size of a small sphere that can fit through the gap formed by three mutually contacting large spheres (this largest small sphere size occurs at diameter ratio $\alpha = 2/3^{1/2} - 1 \approx 0.155$).

Even though very few or no small spheres are incorporated in the jammed backbones of binary MRJ packings at $\alpha = 0.100$ before the peak in density at $x = 0.9968$, this does not mean that the small spheres have no effect on the structure and contact network of the large spheres. Surprisingly, the presence of small spheres tends to *reduce* the packing fraction of the jammed backbone of large spheres at values of x just below the x at which $\phi_{\mathrm{MRJ}}(0.100,x)$ is at a maximum. This

is strong evidence that the structure of binary MRJ packings of spheres differs fundamentally from that of monodisperse MRJ packings. Notably, binary MRJ packings are never (for the values of α studied) simply monodisperse MRJ packings of spheres with small spheres in the interstices, even when there are no small spheres present in a jammed backbone of only large spheres.

IV. PAIR CORRELATION FUNCTIONS AND CONTACT NUMBERS

Packing pair correlation functions $g_2(r)$ and detailed jammed-sphere contact distributions can provide deeper insight into packing structure. For the binary MRJ packings studied, the structural change that appears as x varies at fixed α is clearly evident in the short-range behavior of the $g_2(r)$. In addition, the $g_2(r)$ indicate a preference in higher-density packings for collinear arrangements of groups of three sphere centers when the three include both small and large spheres.

The pair correlation function $g_2(r)$ of a configuration of points (sphere centers) in $\mathbb{R}^3$ is proportional to the probability density of finding an expected number of points in a volume element $4\pi r^2 dr$ at distance r from an arbitrary point. For an ideal gas, $g_2(r) = 1$ for all r; for a disordered packing, it decays to unity as r increases. The average pair correlation function at small r gives details about pair distances in average local arrangements of the centers of spheres.

For comparative purposes, we present monodisperse MRJ packing average pair correlation functions and contact distributions before their binary counterparts. Figure 9 details the average pair correlation function $g_2(r)$ (for $r \leqslant 3.25$) and contact distribution calculated from 100 packings of 1000 identical spheres employing a contact tolerance of $t = 10^{-6}$ [86]. We report here the average rattler concentration found by the TJ algorithm for the 100 monodisperse packings studied in this work: It is $1.62\% \pm 0.26\%$, which is in agreement with a more thorough investigation using the TJ algorithm [80].

Figure 10 includes plots of average pair correlation functions, each calculated for ten 1000-sphere binary packings at various values of α and x. For x much smaller than the point for which the maximum in $\phi_{\mathrm{MRJ}}(\alpha,x)$ at fixed α is achieved, the pair correlation functions calculated for only the large spheres (top two plots of Fig. 10) closely resemble that of a jammed packing of monodisperse spheres. In particular, the upper left plot of Fig. 10 is virtually indistinguishable from the left plot of Fig. 9. This similarity indicates that the packings employed to generate this plot consist primarily of jammed large spheres, with most small spheres present in the interstices as opposed to in the jammed backbone. The upper right plot of Fig. 10 also has these qualitative features, despite that for the larger value of $\alpha = 0.450$, the small spheres do not fit within the interstices created by jammed large spheres. The upper right plot additionally shows a very sharp local maximum at $r = 1.450$, indicating an increased probability of the presence of two large spheres surrounding and in contact with a small sphere such that the centers of all three spheres are collinear.

The preference for collinearity between three spheres is also evident in the bottom two plots of Fig. 10, which display the average pair correlation functions for spheres of both sizes in ten 1000-sphere packings at the maxima in $\phi_{\mathrm{MRJ}}(\alpha,x)$ at $\alpha = 0.450$, $x = 0.800$, and $\alpha = 0.330$, $x = 0.900$, respectively. In these plots, many of the characteristics of monodisperse MRJ packings, e.g., the "split second peak," are not present, indicating a fundamental structural difference between these high-density binary MRJ packings and those at lower densities. Local maxima and apparent discontinuities are observed in the bottom left plot ($\alpha = 0.450$, $x = 0.800$) of Fig. 10 at $r = 1.175$, $r = 1.450$, and $r = 1.725$, corresponding to collinear arrangements of the centers of two adjacent small spheres with one large sphere, either two small spheres sandwiching a large sphere or two large spheres sandwiching a small sphere, and two adjacent large spheres with one small sphere, respectively.

These collinear arrangements are also represented for $\alpha = 0.330$ and $x = 0.900$, as shown in the bottom right plot of Fig. 10, with local maxima and apparent discontinuities at $r = 0.995$, $r = 1.330$, and $r = 1.665$, respectively. The plot in Fig. 11, an average cross-correlation function proportional to

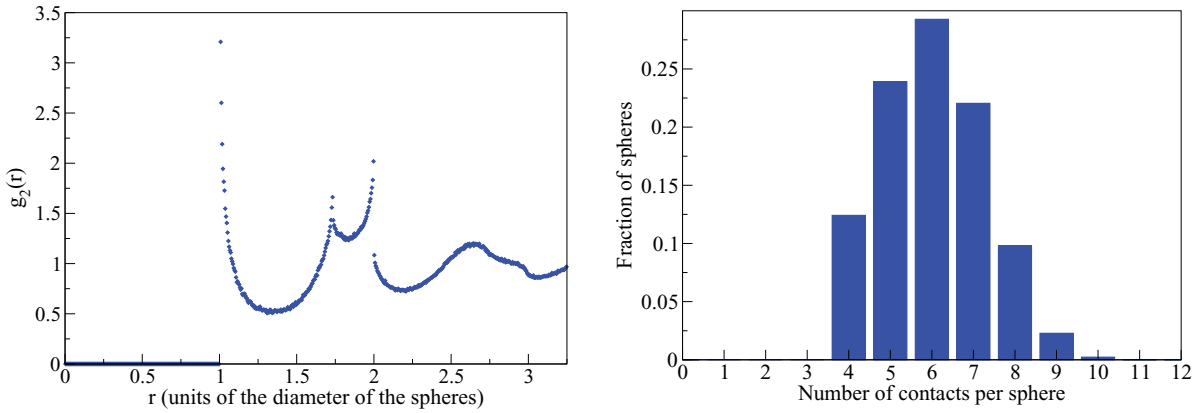

FIG. 9. (Color online) Plots of average pair correlation function (left) and average contact histogram (right) calculated from 100 strictly jammed packings of 1000 monodisperse spheres. In the left figure, the bin ($1.0 < r \leqslant 1.005$) including nearest-neighbor contacts is not shown; its value is 83.92. In the right figure, the average fraction of jammed spheres exhibiting the specified number of contacts is plotted, while the 1.62% of spheres that are rattlers are not. There were no spheres with 12 contacts, and only 0.0059% of jammed spheres exhibited 11 contacts.

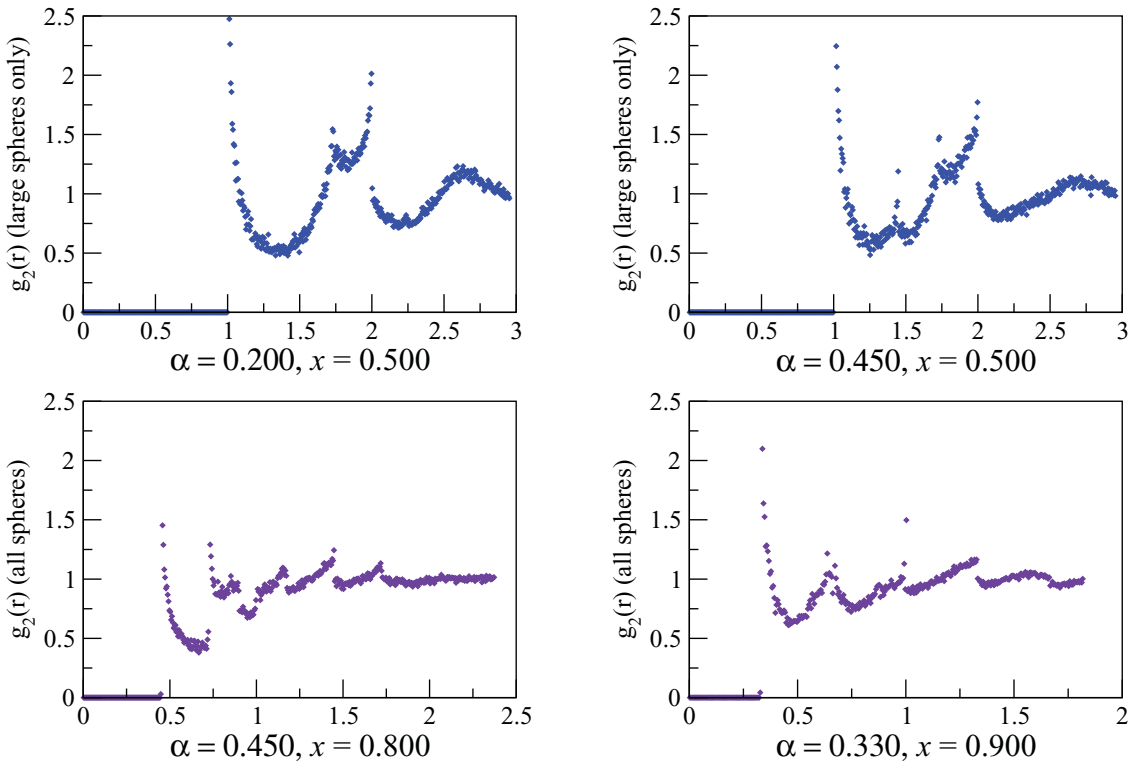

FIG. 10. (Color online) Plots of average pair correlation functions each calculated from ten 1000-sphere packings, where the x axis in each figure is in units of the diameter of the large spheres. The top two figures are pair correlation functions calculated considering only the large spheres in the packings, whereas the bottom two are calculated considering all spheres. In each figure, the bins (of width 0.005 in r) including nearest-neighbor contacts are not shown. In the top left image, the value not shown at $r = 1.0$ is 83.57; in the top right image, the value is 78.16. In the bottom left image, the values not shown are at $r = 0.450$, $r = 0.725$ and $r = 1.0$, with values 33.46, 22.81, and 3.37; in the bottom right image, they are $r = 0.330$ and $r = 0.665$ with values 36.30 and 12.06, respectively.

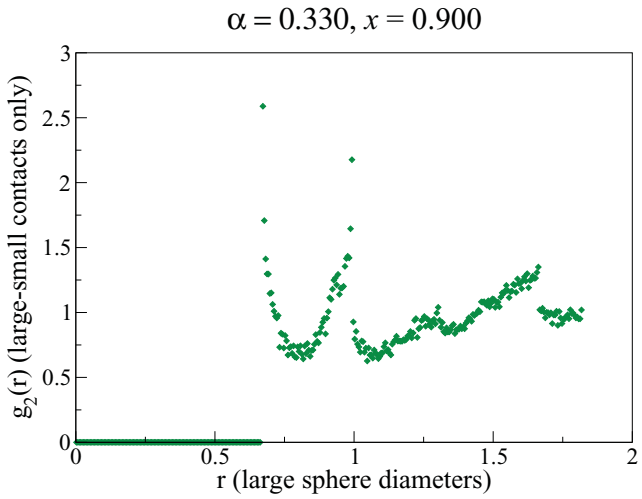

FIG. 11. (Color online) Average cross-correlation function representing large-small sphere center distances calculated from ten 1000-sphere binary packings at $\alpha = 0.330$ and $x = 0.900$. The bin $0.665 \leqslant r < 0.670$ including nearest-neighbor contacts is not shown; it has the value 63.05. Note the local maxima at $r = 0.995$ and $r = 1.665$, indicating an increased probability of collinear arrangements of the centers of two small spheres and one large sphere and of two large spheres and one small sphere, respectively.

the probability density of finding a given distance r between the centers of pairs of spheres of different sizes, highlights that the peak at $r = 0.995$ for packings at $\alpha = 0.330$ and $x = 0.900$ is due to collinear arrangements of the centers of two small spheres and one large sphere, as opposed to arrangements of two contacting large spheres (distance of 1.000) or four contacting small spheres (distance of 0.999). This is also evidence of collinear arrangements of two small spheres and one large sphere in the $g_2(r)$ studied at $\alpha = 0.150$ and $\alpha = 0.100$, though at $\alpha = 0.100$, this is only the case for $x \geqslant 0.997$, probably because no jammed small spheres are present in $\alpha = 0.100$ packings for $x < 0.997$.

We also study the average number and types of contacts per jammed sphere. Past works studying coordination numbers [74,87] have found that the number of large sphere contacts at fixed α increases as x increases, at first slowly and then rapidly roughly when small spheres begin to comprise the volumetric majority of the packing. Studying contact numbers, we also see this behavior, as is illustrated in the bottom three plots of Fig. 12, histograms of average number of contacts per large sphere at $\alpha = 0.200$ and various values of x. In addition, we find in the packings studied that the number of contacts per small sphere never exceeds six. The number is 4 at small x for $\alpha = 0.150$, 0.200, 0.330, and 0.450 and then moves quickly toward (but never exceeds) 6 roughly when the small spheres

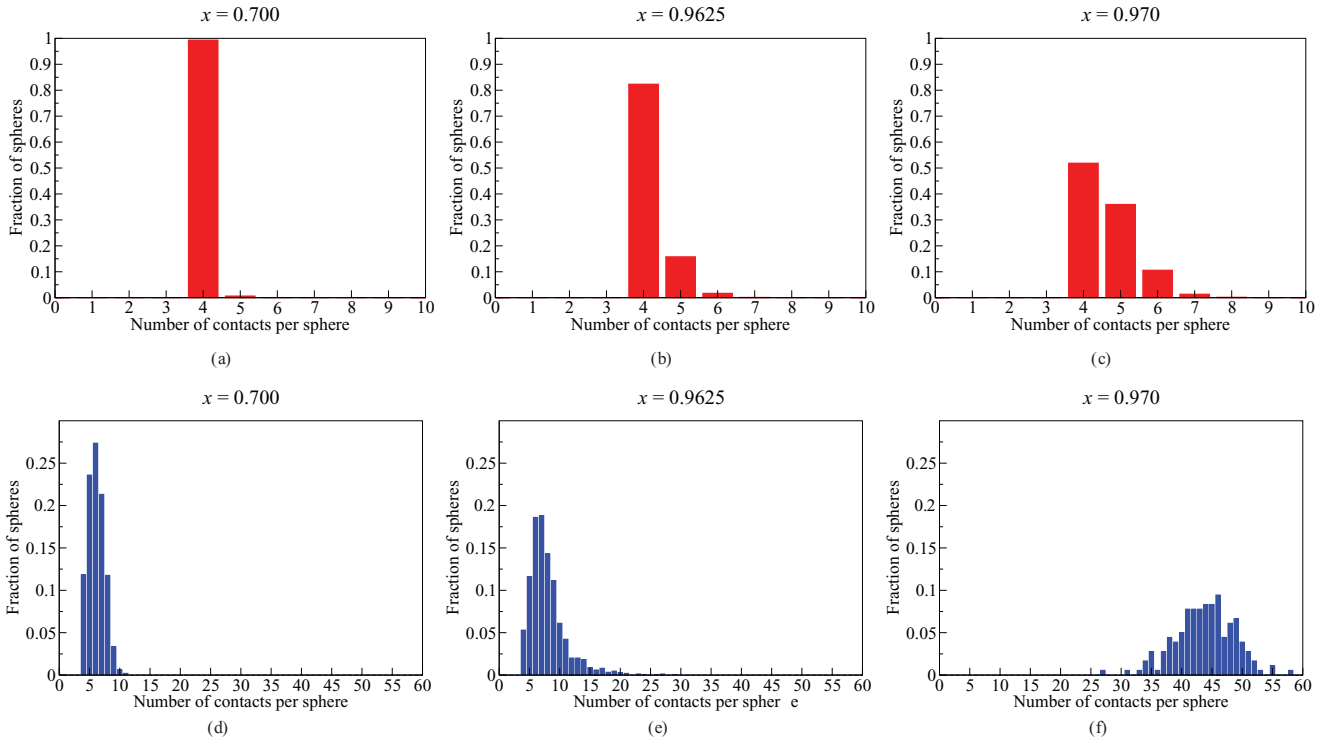

FIG. 12. (Color online) Histograms depicting the average fractions of jammed spheres with specified numbers of contacts for $\alpha = 0.200$ and $x = 0.700$ [(a) and (d)], $x = 0.9625$ [(b) and (e)], and $x = 0.9700$ [(c) and (f)]. Plots (a), (b), and (c) each represent the average over 10 packings of the fractions of jammed small spheres with specified contact numbers, and plots (d), (e), and (f) each represent average fractions for the jammed large spheres.

begin to form the numeric majority of the jammed backbone of the packing. The upper three plots of Fig. 12 illustrate this behavior for $\alpha = 0.200$ at various values of x.

Detailed contact distributions can also reveal information about clustering in strictly jammed packings. For example, at $\alpha = 0.200$ and $x = 0.700$ for small sphere contacts (upper left plot of Fig. 12), each small sphere has one small-small contact and three small-large contacts, indicating that all jammed small spheres are present in "dipole" clusters of two spheres. This is roughly the case also for $x = 0.9625$, though some larger clusters are present as well. However, at $x = 0.970$ (the point at which the jammed backbone density increases dramatically for $\alpha = 0.200$), there are an average of three small-small contacts per jammed small sphere and one or two (but no more than three) small-large contacts, suggesting percolation of small and possibly also large spheres (as seen in Fig. 1). This notion is supported by the large-sphere contact distribution for $\alpha = 0.200$ and $x = 0.970$, shown in the bottom right plot of Fig. 12, which depicts an average of about 44 sphere contacts per large sphere, including an average of 40 small-large contacts and 4 large-large contacts. For $\alpha = 0.150$ and $x < 0.989$, contact distributions reveal that clusters of four jammed small spheres are preferred, suggesting that clusters including large and small spheres require four spheres at the smaller $\alpha = 0.150$ relative size in order for jamming to occur.

V. CONCLUSION AND DISCUSSION

We have generated exactly isostatic, mechanically stable binary sphere packings over the broadest spectrum of average densities $0.634 \leqslant \phi_{\mathrm{MRJ}}(\alpha,x) \leqslant 0.829$ for $\alpha \geqslant 0.100$, with average packing fractions for MRJ packings at certain α and x surprisingly approaching those of the densest known packings. Nevertheless, the packing fraction of the jammed packing backbones appear to be roughly constant over the majority of the area of the α-x plane, even when small spheres are present in the backbones in significant numbers. The latter finding is unexpected, in particular because the jammed backbones of the densest packings of binary spheres exhibit vastly different packing fractions as α and x vary [20,70].

Rather than a linear, "triangular" shape in $\phi_{\mathrm{MRJ}}(\alpha,x)$ as a function of x at fixed α, we observe proportionality of $\phi_{\mathrm{MRJ}}(\alpha,x) \propto a + bx/(c - x)$ over a range of x, with this proportionality for the smallest values of α studied extending very near to the maximum in $\phi_{\mathrm{MRJ}}(\alpha,x)$. This sharp spike in density has practical implications for the development of granular composites such as solid propellants, concrete, and ceramics. For example, the burning rate of ammonium-perchlorate solid propellants is influenced by the size and size distribution of ammonium-perchlorate particles through particle packing [88]. Specifically tailoring the size and polydispersities of particles to achieve maximal densities corresponding precisely to the peaks identified in this work could lead to substantial performance improvements. This is also the case for concrete, the mechanical strength of which can depend exponentially on its density [89]. The cost of producing most concrete also depends heavily on the amount of cement used to fill the gaps between granular aggregates such as sand and gravel, meaning that carefully chosen aggregate sizes could lead to decreased production costs. With respect to ceramics, in several industrial

processes such as sintering and ceramic formation, there is interest in increasing the density and number of contacts of the powder particles to be fused [90].

We have also studied pair correlation functions and detailed contact distributions of the packings, the latter study being possible given the ability of the TJ algorithm to generate precisely strictly jammed packings. Binary MRJ packing pair correlation functions indicate a preference for collinearity among three-sphere arrangements consisting of both small and large spheres. They also indicate a fundamental change in packing structure as x increases at fixed α, which is exemplified by a sharp increase in the presence of small spheres in packings' backbones. Additionally, contact distributions indicate the presence of two-sphere jammed small-sphere clusters in packings of binary spheres at smaller values of α and x, where at the smallest values of α studied and x less than the x at which the peak in $\phi_{\mathrm{MRJ}}(\alpha,x)$ occurs, small spheres in two- or four-sphere clusters are the only spheres present in the jammed backbone.

In future work, we will study binary MRJ packings at smaller values of α. We will investigate polydisperse packings of more than two types of spheres, for which we expect an even broader density range and the presence of more intricate MRJ structures. We will also introduce order metrics capable of comparing the degree of order in the densest known binary packings to the MRJ-like packings studied in this work. Order metrics will also be computed for larger (greater than 1000 spheres) monodisperse strictly jammed exactly isostatic packings, and finite-size effects in order metrics, number of rattlers, and other packing descriptors will be investigated.

Quasi-long-range pair correlations with asymptotic scaling of $-1/r^4$ have been shown to be a unique signature of MRJ packings of monodisperse spheres [57,58] as well as jammed binary sphere packings [60,91,92] and MRJ packings of nonspherical particles [33,92], when the corresponding structure factor $S(k)$ is appropriately generalized. The latter quantity for monodisperse MRJ sphere packings and the so-called spectral density $\chi(k)$ for polydisperse packings and packings of nonspherical objects go to zero linearly as the wave number k tends to zero, translating to the aforementioned quasi-long-range pair correlations. Any system in which these spectral functions vanish in the infinite-wavelength limit are called hyperuniform [59], since their large-scale density or volume-fraction fluctuations vanish. In future work it will be interesting to determine the possible set of (α,x) consistent with MRJ binary sphere packings that are simultaneously hyperuniform.

ACKNOWLEDGMENTS

This work was supported by the MRSEC Program of the National Science Foundation under Award No. DMR-0820341. The simulations of strictly jammed binary sphere packings using the TJ algorithm were performed in part on computational resources supported by the Princeton Institute for Computational Science and Engineering (PICSciE) and the Office of Information Technology's High Performance Computing Center and Visualization Laboratory at Princeton University. S.T. gratefully acknowledges the support of a Simons Fellowship in Theoretical Physics, which has made possible his sabbatical leave this entire academic year. He also thanks the Department of Physics and Astronomy at the University of Pennsylvania for their hospitality during his stay there.

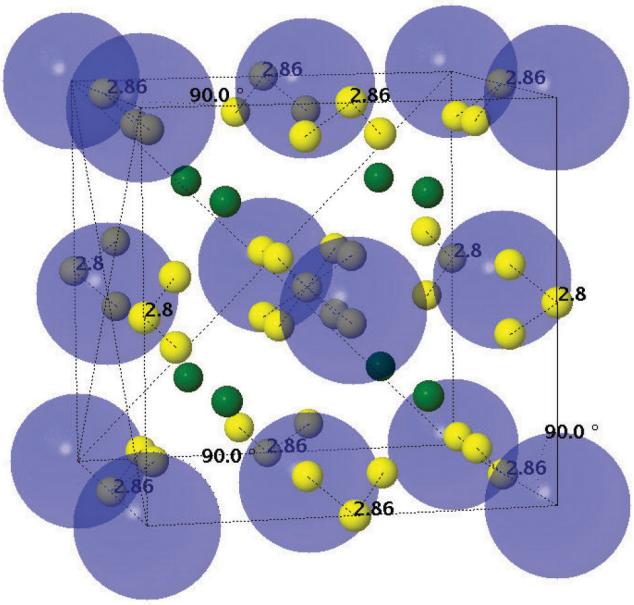

FIG. 13. (Color online) This packing at $\alpha = 0.2195$ and $x = 11/12$ belongs to the same family (in terms of unit cell symmetry and concentrations) as the densest known packing of binary spheres at $\alpha = 0.200$ and $x = 11/12$. In this image, small spheres in tetrahedral interstices are shown in green (dark gray) and small spheres in octahedral interstices are shown in yellow (light gray). The fundamental cell of this (11-1) alloy belongs to the tetragonal lattice system.

APPENDIX A: DENSEST KNOWN BINARY PACKINGS

The densest known binary packings of spheres are composed of separated regions of both binary and monodisperse phases. The binary phases include nearly 20 different families of ordered alloys, where the term "alloy" is used to apply to structures with more than one component in fixed relative concentration, e.g., a binary packing with $\alpha = 0.200$ and $x = 11/12$. The currently known densest packing at $\alpha = 0.200$, $x = 0.970$ is composed of two phases. One of these is a binary alloy consisting of 11 small spheres for every large sphere packed in the (11-1) family illustrated in Fig. 13, and the other consists of close-packed (e.g., fcc or hcp) monodisperse small spheres exhibiting packing fraction $\phi = \pi/\sqrt{18} = 0.7405\ldots$ [20,70].

APPENDIX B: A LINEAR FUNCTIONAL RELATION BETWEEN PACKING FRACTION AND ϕ_S

The functional forms for $\phi_{\mathrm{MRJ}}(\alpha,x)$ and $\phi_{\mathrm{MRJ}}(\alpha,x_V)$ represented by Eqs. (2) and (4), respectively, are also mathematically interesting from the perspective of another measure of volume fraction, ϕ_S. A simpler version of these forms is implied by a linear relation between average packing fraction

and ϕ_S for a fixed value of α, where ϕ_S is the volume fraction of *space* covered by only the small spheres [93].

A proposed linear relation between ϕ_S and average packing fraction can be written as

$$\phi_{\mathrm{MRJ}}(\alpha,\phi_S) = a + h(\alpha)\phi_S, \tag{B1}$$

where the functional dependence of the average ϕ_S for MRJ binary packings on α and x can be written in terms of $\phi_{\mathrm{MRJ}}(\alpha,x)$ as

$$\phi_S(\alpha,x) = \frac{\alpha^3 x}{(1/\phi_{\mathrm{MRJ}}(\alpha,x))(\alpha^3 x + 1 - x)}. \tag{B2}$$

Combining Eqs. (B1) and (B2) permits an implicit form to be written for average packing fraction,

$$\phi_{\mathrm{MRJ}}(\alpha,x) = a + h(\alpha)\frac{\phi_{\mathrm{MRJ}}(\alpha,x)\alpha^3 x}{\alpha^3 x + 1 - x}, \tag{B3}$$

which can be solved explicitly for x to give

$$\phi_{\mathrm{MRJ}}(\alpha,x) = a + \frac{a h(\alpha)\alpha^3 x}{1 - x + \alpha^3 x[1 - h(\alpha)]}. \tag{B4}$$

If $h(\alpha)$ were equal to unity in Eq. (B1), then from a density perspective, it would be tempting to accept the conceptual picture of binary packings as MRJ packings of large spheres with small spheres placed in the void spaces. However, this is not an accurate picture, as small spheres are present in increasing numbers (as a function of x) in the jammed backbone of MRJ binary packings, as demonstrated in Sec. III. Indeed, $h(\alpha)$ is not unity, and it is not clear at this point that the linear form suggested by Eq. (B4) precisely describes the data even with a slope $h(\alpha) \neq 1$, though from our research it does appear to provide a good fit. Figure 14 illustrates the best linear fit obtained of average packing fraction as a function of ϕ_S for the $\alpha = 0.200$ packings studied in this work. For this fit, $h(0.200) = 0.934$.

The linear fit to the data presented in Fig. 14 is not quite as precise as the fits of average packing fraction to the forms of Eqs. (2) and (4) when the average packing fraction is depicted as a function of x and x_V, respectively. However, if the functional form represented by Eq. (4) is considered a sufficiently precise fit to the data, then the constants $b(\alpha)$ and $c(\alpha)$ in Eq. (2) can be written only in terms of one free parameter $h(\alpha)$ as

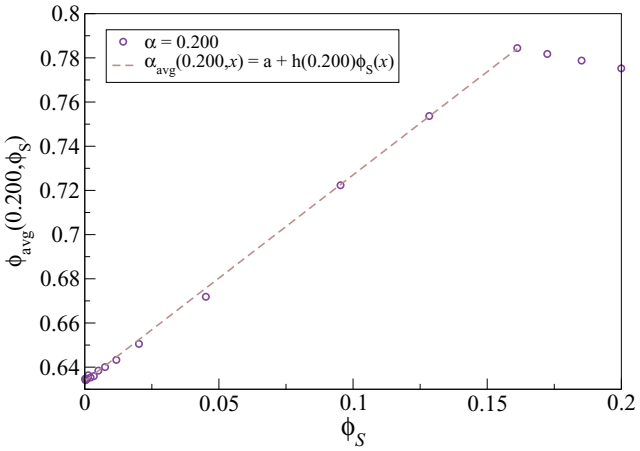

FIG. 14. (Color online) Plot of the average packing fraction obtained at $\alpha = 0.200$ for the values of x presented in Figs. 4 and 5. Each data point represents an average of 10 packings, and the measured standard deviation is slightly smaller than the size of the symbols. The dashed line is a least-squares linear fit of the form of Eqs. (B3) and (B4) to the data from $\phi_S = 0$ to $\phi_S = 0.1612$ (equivalent to the range $x = 0$ to $x = 0.970$). The fit exhibits a slope $h(0.200) = 0.934$ and an R^2 of 0.9993.

$$b(\alpha) = \frac{a\alpha^3 h(\alpha)}{1 - \alpha^3 + \alpha^3 h(\alpha)}, \tag{B5}$$

$$c(\alpha) = \frac{1}{1 - \alpha^3 + \alpha^3 h(\alpha)}. \tag{B6}$$

This indicates that there is an additional free parameter in the fits represented by Eqs. (2) and (4) as functions of x and x_V as compared to the linear fit as a function of ϕ_S presented in Eq. (B1) and suggests that the increased precision in the fits as functions of x and x_V could simply be the result of including the additional parameter. Further investigations will be needed to determine whether this is the case.

[1] R. Zallen, *The Physics of Amorphous Solids* (John Wiley & Sons, New York, 1983).
[2] J. P. Hansen and I. R. McDonald, *Theory of Simple Liquids,* 3rd ed. (Academic Press, Amsterdam, 1986).
[3] I. C. Kim and S. Torquato, J. Appl. Phys. **69**, 2280 (1991).
[4] P. M. Chaikin and T. C. Lubensky, *Principles of Condensed Matter Physics* (Cambridge University Press, Cambridge, 1995).
[5] S. Torquato, *Random Heterogeneous Materials* (Springer-Verlag, New York, 2002).
[6] T. I. Zohdi, Mech. Mater. **38**, 969 (2006).
[7] A. Mejdoubi and C. Brosseau, J. Appl. Phys. **101**, 084109 (2007).
[8] N. J. A. Sloane, R. H. Hardin, T. D. S. Duff, and J. H. Conway, Discrete Comput. Geom. **14**, 237 (1995).
[9] J. H. Conway and N. J. A. Sloane, *Sphere Packings, Lattices and Groups* (Springer, Berlin, 1998).
[10] H. Cohn and N. Elkies, Ann. Math. **157**, 689 (2003).
[11] T. C. Hales, Ann. Math. **162**, 1065 (2005).
[12] S. Torquato and F. H. Stillinger, Exp. Math. **15**, 307 (2006).
[13] A. B. Hopkins, F. H. Stillinger, and S. Torquato, Phys. Rev. E **79**, 031123 (2009).
[14] A. B. Hopkins, F. H. Stillinger, and S. Torquato, J. Math. Phys. **51**, 043302 (2010).
[15] A. B. Hopkins, F. H. Stillinger, and S. Torquato, Phys. Rev. E **81**, 041305 (2010).
[16] A. B. Hopkins, F. H. Stillinger, and S. Torquato, Phys. Rev. E **83**, 011304 (2011).
[17] H. Cohn, Y. Jiao, A. Kumar, and S. Torquato, Geom. Topol. **15**, 2235 (2011).
[18] A. Andreanov and A. Scardicchio, Phys. Rev. E **86**, 041117 (2012).

[19] E. C. Oğuz, M. Marechal, F. Ramiro-Manzano, I. Rodriguez, R. Messina, F. J. Meseguer, and H. Löwen, Phys. Rev. Lett. **109**, 218301 (2012).
[20] A. B. Hopkins, F. H. Stillinger, and S. Torquato, Phys. Rev. E **85**, 021130 (2012).
[21] É. Marcotte and S. Torquato, Phys. Rev. E **87**, 063303 (2013).
[22] J. Schroers, Phys. Today **66**, 32 (2013).
[23] A. Donev, F. H. Stillinger, P. M. Chaikin, and S. Torquato, Phys. Rev. Lett. **92**, 255506 (2004).
[24] Y. Jiao, F. H. Stillinger, and S. Torquato, Phys. Rev. E **79**, 041309 (2009).
[25] R. D. Batten, F. H. Stillinger, and S. Torquato, Phys. Rev. E **81**, 061105 (2010).
[26] S. Torquato and Y. Jiao, Nature **460**, 876 (2009).
[27] S. Torquato and Y. Jiao, Phys. Rev. E **80**, 041104 (2009).
[28] S. Torquato and Y. Jiao, Phys. Rev. E **81**, 041310 (2010).
[29] E. Chen, Discrete Comput. Geom. **40**, 214 (2008).
[30] E. Chen, M. Engel, and S. Glotzer, Discrete Comput. Geom. **44**, 253 (2010).
[31] Y. Kallus, V. Elser, and S. Gravel, Discrete Comput. Geom. **44**, 245 (2010).
[32] J. de Graaf, R. van Roij, and M. Dijkstra, Phys. Rev. Lett. **107**, 155501 (2011).
[33] Y. Jiao and S. Torquato, Phys. Rev. E **84**, 041309 (2011).
[34] R. Kurita and E. R. Weeks, Phys. Rev. E **84**, 030401 (2011).
[35] Y. Jiao and S. Torquato, J. Chem. Phys. **135**, 151101 (2011); S. Torquato and Y. Jiao, Phys. Rev. E **86**, 011102 (2012).
[36] F. Ding and N. V. Dokholyan, Trends Biotech. **23**, 450 (2005).
[37] N. V. Dokholyan, Curr. Opin. Struct. Biol. **16**, 76 (2006).
[38] C. H. Davis, H. Nie, and N. V. Dokholyan, Phys. Rev. E **75**, 051921 (2007).
[39] D. Drasdo and S. Höhme, Phys. Biol. **2**, 133 (2005).
[40] J. L. Gevertz, G. Gillies, and S. Torquato, Phys. Biol. **5**, 036010 (2008).
[41] J. L. Gevertz and S. Torquato, PLoS Comp. Biol. **4**, e1000152 (2008).
[42] G. D. Scott, Nature **188**, 908 (1960).
[43] G. Scott and D. Kilgour, Br. J. Appl. Phys. Ser. **2**, 863 (1969).
[44] J. D. Bernal, Nature **183**, 141 (1959).
[45] J. D. Bernal, Nature **185**, 68 (1960).
[46] G. Parisi and F. Zamponi, Rev. Mod. Phys. **82**, 789 (2010).
[47] S. Torquato and F. H. Stillinger, Rev. Mod. Phys. **82**, 2633 (2010).
[48] J. Finney, Proc. R. Soc. London A **319**, 479 (1970).
[49] J. Bernal and J. Finney, Proc. R. Soc. London A **319**, 495 (1970).
[50] B. D. Lubachevsky and F. H. Stillinger, J. Stat. Phys. **60**, 561 (1990).
[51] B. D. Lubachevsky, F. Stillinger, and E. Pinson, J. Stat. Phys. **64**, 501 (1991).
[52] O. Pouliquen, M. Nicolas, and P. D. Weidman, Phys. Rev. Lett. **79**, 3640 (1997).
[53] S. Torquato, T. M. Truskett, and P. G. Debenedetti, Phys. Rev. Lett. **84**, 2064 (2000).
[54] T. M. Truskett, S. Torquato, and P. G. Debenedetti, Phys. Rev. E **62**, 993 (2000).
[55] A. R. Kansal, S. Torquato, and F. H. Stillinger, J. Chem. Phys. **117**, 8212 (2002).
[56] A. Donev, S. Torquato, and F. H. Stillinger, Phys. Rev. E **71**, 011105 (2005).
[57] A. Donev, F. H. Stillinger, and S. Torquato, Phys. Rev. Lett. **95**, 090604 (2005).
[58] A. B. Hopkins, F. H. Stillinger, and S. Torquato, Phys. Rev. E **86**, 021505 (2012).
[59] S. Torquato and F. H. Stillinger, Phys. Rev. E **68**, 041113 (2003).
[60] L. Berthier, P. Chaudhuri, C. Coulais, O. Dauchot, and P. Sollich, Phys. Rev. Lett. **106**, 120601 (2011).
[61] M. Hejna, P. J. Steinhardt, and S. Torquato, Phys. Rev. B **87**, 245204 (2013).
[62] R. Xie, G. G. Long, S. J. Weigand, S. C. Moss, T. Carvalho, S. Roorda, M. Hejna, S. Torquato, and P. J. Steinhardt, Proc. Natl. Acad. Sci. USA **110**, 13250 (2013).
[63] E. Marcotte, F. H. Stillinger, and S. Torquato, J. Chem. Phys. **138**, 12A508 (2013).
[64] C. S. O'Hern, S. A. Langer, A. J. Liu, and S. R. Nagel, Phys. Rev. Lett. **88**, 075507 (2002).
[65] P. J. Steinhardt, D. R. Nelson, and M. Ronchetti, Phys. Rev. B **28**, 784 (1983).
[66] S. Torquato and F. H. Stillinger, J. Phys. Chem. B **106**, 8354 (2002).
[67] C. F. Schreck, C. S. O'Hern, and L. E. Silbert, Phys. Rev. E **84**, 011305 (2011).
[68] P. Chaudhuri, L. Berthier, and S. Sastry, Phys. Rev. Lett. **104**, 165701 (2010).
[69] Y. Jiao, F. H. Stillinger, and S. Torquato, J. Appl. Phys. **109**, 013508 (2011).
[70] A. B. Hopkins, Y. Jiao, F. H. Stillinger, and S. Torquato, Phys. Rev. Lett. **107**, 125501 (2011).
[71] P. I. O'Toole and T. S. Hudson, J. Phys. Chem. C **115**, 19037 (2011).
[72] S. Torquato and Y. Jiao, Phys. Rev. E **82**, 061302 (2010).
[73] A. Donev, S. Torquato, F. H. Stillinger, and R. Connelly, J. Comput. Phys. **197**, 139 (2004).
[74] K. L. Kristiansen, A. Wouterse, and A. Philipse, Physica A **358**, 249 (2005).
[75] E. Santiso and E. A. Müller, Mol. Phys. **100**, 2461 (2002).
[76] A. S. Clarke and J. D. Wiley, Phys. Rev. B **35**, 7350 (1987).
[77] D. M. E. Thies-Weesie and A. P. Philipse, J. Colloid Interface Sci. **162**, 470 (1994).
[78] R. K. McGeary, J. Am. Chem. Soc. **44**, 513 (1961).
[79] M. Ozawa, T. Kuroiwa, A. Ikeda, and K. Miyazaki, Phys. Rev. Lett. **109**, 205701 (2012).
[80] S. Atkinson, F. H. Stillinger, and S. Torquato (to be published).
[81] H. J. H. Brouwers, Phys. Rev. E **87**, 032202 (2013).
[82] A. Donev, S. Torquato, F. H. Stillinger, and R. Connelly, J. Appl. Phys. **95**, 989 (2004).
[83] A. R. Kansal, S. Torquato, and F. H. Stillinger, Phys. Rev. E **66**, 041109 (2002).
[84] The algorithm does not appear to be very sensitive to changes in maximum step sizes for step sizes smaller than 0.1 large-sphere diameters.
[85] S. Torquato and F. H. Stillinger, J. Appl. Phys. **102**, 093511 (2007).
[86] In a very large packing, different regions of the packing will show some variation in packing fraction and structure. The calculation of average pair correlation function performed in this work assumes that some very large packing includes 100 regions of 1000 spheres that are the independently generated samples used to calculate the average pair correlation functions shown in Fig. 9.

[87] D. Pinson, R. P. Zou, A. B. Yu, P. Zulli, and M. J. McCarthy, J. Phys. D: Appl. Phys. **31**, 457 (1998).

[88] S. Kochevets, J. Buckmaster, T. L. Jackson, and A. Hegab, J. Propul. Power **17**, 883 (2001).

[89] S. Mindess and J. F. Young, *Concrete* (Prentice-Hall, Englewood Cliffs, NJ, 1981).

[90] W. D. Kingery, H. K. Bowen, and D. R. Uhlmann, *Introduction to Ceramics,* 2nd ed. (Wiley-Interscience, New York, 1976).

[91] C. E. Zachary, Y. Jiao, and S. Torquato, Phys. Rev. Lett. **106**, 178001 (2011).

[92] C. E. Zachary, Y. Jiao, and S. Torquato, Phys. Rev. E **83**, 051308 (2011).

[93] The variable ϕ_S is not to be confused with x_V. While ϕ_S is the fraction of small-sphere volume to the volume of space including all spheres and voids, x_V is the relative volume fraction of small spheres, i.e., where the denominator in the fraction excludes void space.